Characterizing Double and Triple Laser Beam Interference Patterns in the Context of Trapping Atoms for Quantum Computing

A Senior Project

presented to

the Faculty of the Dept. of Physics California Polytechnic State University,

San Luis Obispo

In Partial Fulfillment

of the Requirements for the Degree

Bachelor of Science

by

Ian E. Powell

January, 2015

©2015 Ian Powell

Abstract

We propose two optical neutral atom traps for quantum computing involving the intersection of two or three laser beams. We simulate both the intensity and the potential energy of the interference pattern. From these simulations we create animations of how the potential energy and intensity change with varying angles of separation between the laser beams in the system. We parameterize lines through our interference pattern and fit simple harmonic oscillator potential energies to the potential energy wells calculated to characterize our interference pattern's atom trapping capabilities. Finally, we investigate a possible quantum entanglement routine by observing how the geometry of both the intensity pattern and potential energy changes in our different animations. For the case of the double beam trap with different beam waists at $\theta = \pi/2$, we found $\eta = 41.8$ KHz and $\Delta U_{trap} = 0.042$ mK for BEC atoms, and $\eta = 41.2$ KHz and $\Delta U_{trap} = 12.4$ mK for MOT atoms. For the case of the triple beam trap with all beams having equal parameters at $\theta = \pi/2$, $\theta_2 = 0$, and $\gamma = 3\pi/4$ we found $\eta = 8.00$ KHz and $\Delta U_{trap} = 0.62$ mK.

CONTENTS

LIST OF FIGURES

LIST OF TABLES

I. INTRODUCTION

The field of quantum computing has received a great deal of attention in the physics community due to its exciting prospective applications and recent progress made in constructing systems with characteristics that allow for the formation of so called "qubits." A qubit, or a quantum bit, represents a two-level, quantum mechanical system. Canonical examples of a qubit are a photon's polarization–be it linearly horizontal or linearly vertical–or an electron's spin state–where down and up, or horizontal and vertical correspond to 0 and 1 in terms of binary. The difference, however, between a qubit and a classical bit is the qubit's ability to be in both 0 and 1 simultaneously–a superposition of up and down for the example of the electron's spin. Quantum bits also have the ability to be "entangled" with other quantum bits; this quantum entanglement is a physical phenomenon that occurs when the quantum state of each qubit cannot be described independently from one another–thus, a change in the quantum state of one qubit would have an effect on the quantum state of the other qubit. These properties of superposition and quantum entanglement differentiate quantum computing from its classical counterpart.

David DiVincenzo, while at IBM, famously developed a list of requirements to construct quantum computer. The "DiVincenzo Criteria" [1] are: (1) the system must have a large number of well defined qubits, (2) initialization to a known state for the system must be easily performed, (3) a universal set of quantum logic gates must be developed, (4) qubit-specific measurements must be able to be performed, and (5) long coherence times must exist for the qubits in the system–where coherence time describes how long a quantum state can exist on average before being perturbed, altered by the environment.

Many different types of systems show promise in fulfilling said criteria–for example, solid-state systems in which spin states of electrons or nuclei represent the qubits have promise in their scalability, due to extensive research done on the miniaturizing of semiconductors. Superconducting systems have shown promise in quantum information processing due to the ease of fabricating larger systems. It is, however, in cold neutral atom systems that qubits (atoms) have some of the longest coherence times–offering promise for storing information for longer periods of time. With this longer information storage time we gain the ability to complete many logical gate operations before a qubit's state decoheres.

Qubit storage for cold neutral atom quantum computing is possible by means of creating

cleverly designed light traps. An example of such an optical atom trap are "optical tweezers." In 1970 Arthur Ashkin [2] first trapped micron-sized particles in a tightly focused laser beam (the tweezers). This method of trapping has seen a great deal of success in microbiology; for example DNA's force extension relationship can be determined by stretching the DNA via manipulation of the beam[3]. Another way to create an optical atom trap is to simply create walls of laser light that form a box; with the correct laser frequency tuning atoms will be trapped in the center of the box where there is a dark spot[4]. Optical lattices may also trap atoms–an optical lattice is created by the interference of counter-propagating laser beams, creating a periodic structure of bright and dark spots where atoms may be trapped[4]. The diffraction pattern of light behind a pinhole can also act as an atom trap. The sequence of bright and dark spots that form behind the pinhole offer considerable trapping parameters in all three dimensions of movement[5]. Note that this is not a complete list of all optical atom traps, nor one that highlights traps that are more favorable than others–it is merely a brief overview of different mechanisms that may be used to trap atoms using laser light.

This paper concerns itself with utilizing the interference pattern of two or three laser beams intersecting for trapping atoms. For the instance of two counter-propagating beams: nodal and antinodal planes are created periodically in the region of overlap due to wave superposition. Furthermore, varying the angle between the beams alters the separation distance and orientation of these dark and bright trapping planes (see Fig. 1).

By introducing a difference in beam size between the beams, one beam will create a "wall" around its counterpart–thereby allowing the system to trap atoms in three dimensions as this third dimension is now confined due to the newly created light wall. Introducing a third beam results in tighter traps, resulting in better confinement and trapping time of atoms. We first investigate the relationships between the trapping parameters of the potential energy wells created by these systems and the angles of separation, polarization, difference in beam size, and power of the laser beams. Finally, we investigate a possible entanglement routine and how it would allow entanglement to propagate through the system.

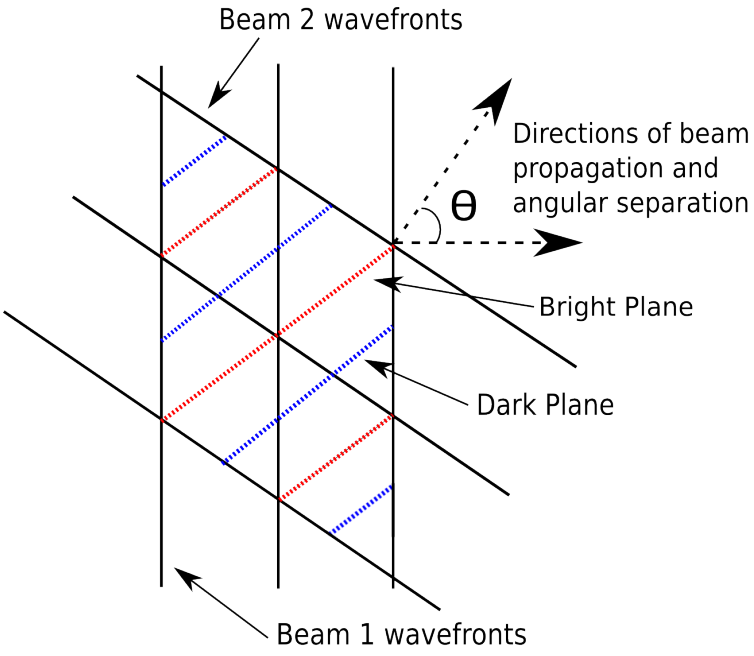

FIG. 1. Visualization of the interference of two laser beams at an angle θ.

II. THEORY

A. Optical Dipole Traps

The light traps used in cold, neutral atom quantum computing are called "dipole traps." The frequency of the trapping laser is detuned from an atomic resonance frequency–meaning that the beam is tuned slightly off of the laser frequency that would excite the target atom to a given energy level–thus the atoms do not absorb laser photons. The electric field of the laser thereby induces a dipole in the atoms that either repels them from or attracts them to brighter spots of laser light. There are two different types of detuning: red and blue. Red detuning describes when the laser beam frequency is tuned slightly below the target atomic energy, and blue detuning describes when the laser beam is tuned slightly above the target atomic energy. In the case that our laser beams are red detuned the atoms will be attracted to the brightest spots in our trap, and for the case that our laser beams are blue detuned the atoms will be attracted to the darkest spots in the trap. Atoms are typically first cooled in a Magneto-Optical Trap (MOT) before being trapped in the laser light, as the kinetic energy of hot atoms is enough to supersede that of the potential energy well created by the

trapping laser beam system.

What follows is a brief summary, for details see [6]. When a polarizable atom or molecule is introduced into an electric field the potential-energy operator for the light-atom interaction is given by

$$\hat{U}(\vec{r}) = -\frac{1}{4}\vec{E_0}^*(\vec{r})\hat{\alpha}\vec{E_0}(\vec{r}), \tag{1}$$

where $E_0(\vec{r})$ is the amplitude of the electric field, with $\vec{E}(\vec{r},t) = Re[\vec{E_0}(\vec{r})e^{-i\omega t}]$, $\hat{\alpha}$ is the polarizability tensor, and ω is the angular frequency of the laser light. The polarizability tensor's components written in a spherical basis are

$$\hat{\alpha}_{q',q} = (-1)^{q'}\sum_{F'}\left[\alpha_{0,F'F}f_{F'F}\sum_{m}\left(c^{F,1,F'}_{m+q-q',q',m+q}c^{F,1,F'}_{m,q,m+q}\left|F,m+q-q\right\rangle\left\langle F,m\right|\right)\right], \tag{2}$$

where q' and $q = \pm 1{,}0$ are the spherical basis components, $\alpha_{0,F'F}$ is the characteristic polarizability scalar, $f_{F'F}$ is the relative oscillator strength of the $F \to F'$ hyperfine transition, and c is the Clebsch-Gordan coefficient for the $F,m \to F',m+q$ dipole transition and related to the $F',m+q \to F,m+q-q'$ dipole transition respectively. The characteristic polarizability scalar is given by

$$\alpha_{0,F'F} = -\frac{\left|\left\langle J'\right|\left|d\right|\left|J\right\rangle\right|^2}{\hbar\Delta_{F'F}}, \tag{3}$$

where $\Delta_{F'F}$ is the laser's angular frequency detuning from the $F \to F'$ transition, and $\left\langle J'\right|\left|d\right|\left|J\right\rangle$ is the reduced dipole matrix element for the $J \to J'$ fine structure transition. To calculate this expression in SI units we utilize the following relationship:

$$\alpha_{0,F'F} = -\frac{3\lambda^3}{32\pi^3}\frac{\Gamma}{\Delta_{F'F}}1.11\times 10^{-10}\frac{\mathrm{Jm}^2}{\mathrm{V}^2}, \tag{4}$$

where Γ is the linewidth of the energy level of the atom being trapped. The linewidth describes the uncertainty of exactly what the energy level is and is typically on the order of MHz in atoms like ^{87}Rb. In our examples we use -10 000 Γ for red laser detuning–meaning the laser beam frequency is 10 000 Γ below the target atomic resonance–and 1 000 Γ for blue laser detuning. Finally, the relative oscillator strength is given by

$$f_{F'F} = (2J'+1)(2F+1)\left|\begin{Bmatrix} F' & I & J' \\ J & 1 & F \end{Bmatrix}\right|^2, \tag{5}$$

where the curly braces term is the six-J symbol, and I is the nuclear spin quantum number.

To calculate the diabatic potential energy for a given atom's F, m_F state we determine the expectation value of the potential energy operator:

$$U_{F,m_F} = \langle F, m_F | \hat{U} | F, m_F \rangle . \tag{6}$$

We then substitute Equation (1) for the potential energy operator into this expression to yield

$$U_{F,m_F} = -\frac{1}{4} \sum_{q',q} E^*_{0q'} E_{0q} \hat{\alpha}_{q',q}, \tag{7}$$

where $E_{0q',q}$ are the spherical components of the electric field amplitude with $q', q = \pm 1, 0$ corresponding to right and left circular light polarization, and linear polarization respectively, which we can simplify by exploiting orthonormality and the relationships between Clebsch-Gordon coefficients to yield

$$U_{F,m_F} = -\frac{1}{4} \sum_{q} (-1)^q |E_{0q}|^2 \sum_{F'} \alpha_{0,F'F} f_{F'F} (c^{F,1,F'}_{m_F,q,m_F+q})^2. \tag{8}$$

To write the electric field amplitude in a spherical basis we utilize the spherical unit vectors

$$\hat{e}_{-1} = \frac{\sqrt{2}}{2}(\hat{i} - i\hat{j}) \tag{9}$$

$$\hat{e}_o = \hat{k} \tag{10}$$

$$\hat{e}_{+1} = -\frac{\sqrt{2}}{2}(\hat{i} + i\hat{j}), \tag{11}$$

where $\hat{i}$, $\hat{j}$, $\hat{k}$ are the typical Cartesian unit vectors along x, y, and z respectively. Thus we can write the electric field vector as

$$\vec{E_0} = E_{0-1}\hat{e}_{-1} + E_{00}\hat{e}_0 + E_{0+1}\hat{e}_{+1}, \tag{12}$$

where

$$E_{0-1} = \frac{1}{\sqrt{2}}(E_{0x} + iE_{0y}), \tag{13}$$

$$E_{00} = E_{0z}, \tag{14}$$

$$E_{0+1} = \frac{1}{\sqrt{2}}(-E_{0x} + iE_{0y}). \tag{15}$$

Finally, after the potential energy has been found, we convert it from units of Joules to units of Millikelvin by the relation

$$U_{F,m_F}(mK) = 1000 \frac{2}{3k_B} \frac{2I_0}{\epsilon_0 c} U_{F,m_F}, \tag{16}$$

where k_B is Boltzmann's constant, I_0 is the intensity of at the center of the laser beam, c is the speed of light, and ϵ_0 is the permittivity of free space.

B. Gaussian Laser Beams

A Gaussian beam traveling along the z-axis has an electric field described by the cylindrically symmetric expression

$$E(r,z,t) = E_0 \frac{w_0}{w(z)} e^{-r^2/w(z)^2} e^{ikr^2/(2R(z))} e^{-i\tan^{-1}(z/z_0)} e^{i(kz-\omega t+\phi)}, \tag{17}$$

where E_0 is the electric field amplitude at the center of the beam, z is the distance traveled along the z-axis–the axis which the beam is traveling along–z_0 is the Rayleigh range–the distance spanned along the z-axis from the beam waist to where the beam radius has increased by a factor of $\sqrt{2}$, w_0 is the beam waist–the radial size of the narrowest portion of the beam–ϕ is the phase, r is the radial distance from the center of the beam, R is the radius of curvature of a wavefront, k is the wave number, ω is the angular frequency, and w is the beam radius. The beam radius is defined as the radial distance at which the intensity has dropped to $1/e^2$ of that at the center of the beam; alternatively, it is the radial distance at which the electric field has dropped to $1/e$ of that at the center. The z-dependence of the beam radius can be described by

$$w(z) = w_0 \sqrt{1 + z^2/z_0^2}. \tag{18}$$

z_0 is given by

$$z_0 = \frac{\pi w_0^2}{\lambda}, \tag{19}$$

with λ being the wavelength of the laser. Finally, R is given by

$$R(z) = z(1 + z_0^2/z^2). \tag{20}$$

For a detailed derivation of this expression for the electric field see, for example, *Introduction to Optics.*[7]

III. THE ATOM TRAPS

A. Double Beam Interference Trap

When another Gaussian beam is introduced coordinate system transformations must be taken into consideration as cylindrical symmetry is broken in Equation (14). Here we transfer

to a more favorable Cartesian metric where $r = \sqrt{x^2 + y^2}$. We denote the two beams as the "basis" and "differential" beams where our basis defines our z-axis as its axis of propagation and our differential beam subtends an angle θ between the basis beam's axis and its own beam's z-axis. Thus we define the differential beam's coordinates (x_2, y_2, z_2) in terms of the basis beam's coordinates (x, y, z) by the transformation relations:

$$x_2 = xcos(\theta) + zsin(\theta), \tag{21}$$

$$y_2 = y, \tag{22}$$

$$z_2 = zcos(\theta) - xsin(\theta). \tag{23}$$

The convention here is that the basis beam's axis, z, travels along to the right, x is downward, and y is into the plane, as shown in Fig. 2.

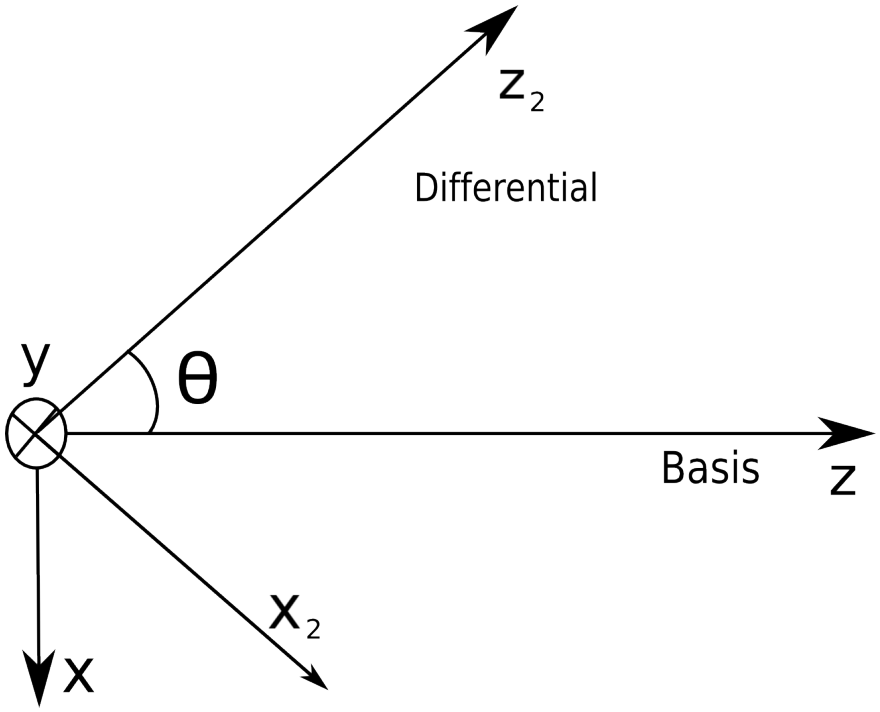

FIG. 2. Coordinate system chosen for the double beam system.

For the total electric field we simply add the component electric fields of each individual beam–for convenience I denote each beam's electric field expression in a component direction, l, as E_{1l} for the basis beam's parameters and E_{2l} for the differential beam's parameters–i.e. $E_{1x} = E(x, y, z, t)$:

$$E_x = E_{1x}(x, y, z) + E_{2x}(x_2, y_2, z_2)cos(\theta), \tag{24}$$

$$E_y = E_{1y}(x, y, z) + E_{2y}(x_2, y_2, z_2) \tag{25}$$

$$E_z = E_{2x}(x_2, y_2, z_2)sin(\theta). \tag{26}$$

The intensity of the interference pattern is given by

$$I = \frac{1}{2}\epsilon_0 c|\vec{E}|^2, \tag{27}$$

which can be expanded out to be written as

$$I = \frac{1}{2}\epsilon_0 c(Re\{E_x\}^2 + Re\{E_y\}^2 + Re\{E_z\}^2 + Im\{E_x\}^2 + Im\{E_y\}^2 + Im\{E_z\}^2), \tag{28}$$

which we then plot to visualize the geometry of the lattice of traps created.

B. Triple Beam Interference Trap

Adding a third beam requires an additional layer of coordinate transformations. The transformation relations for this second differential beam with respect to the basis' coordinates are:

$$x_3 = xcos(\gamma)cos(\theta_2) + zsin(\gamma)cos(\theta_2) - ysin(\theta_2) \tag{29}$$

$$y_3 = zsin(\gamma)sin(\theta_2) + ycos(\theta_2) + xcos(\gamma)sin(\theta_2) \tag{30}$$

$$z_3 = zcos(\gamma) - xsin(\gamma), \tag{31}$$

where γ is the polar angle subtended between the second differential beam and the z-axis, and θ_2 is the azimuthal angular separation between the second differential beam's y-axis with the basis beam's y-axis. We choose y_3 to always be coplanar with x and y for simplicity–see Fig. 3.

Thus when adding the component electric fields of the different beams with the said coordinate system conventions we obtain:

$$E_x = E_{1x}(x, y, z) + E_{2x}(x_2, y_2, z_2)cos(\theta) + E_{3x}(x_3, y_3, z_3)cos(\theta_2)cos(\gamma) + E_{3y}sin(\theta_2) \tag{32}$$

$$E_y = E_{1y}(x, y, z) + E_{2y}(x_2, y_2, z_2) + E_{3x}(x_3, y_3, z_3)cos(\gamma)sin(\theta_2) + E_{3y}cos(\theta_2) \tag{33}$$

$$E_z = E_{2x}(x_2, y_2, z_2)sin(\theta) + E_{3x}(x_3, y_3, z_3)(-sin(\gamma)), \tag{34}$$

see the Appendix for a derivation. We then calculate the interference pattern's intensity using Equation (16) as we did in the two-beam case.

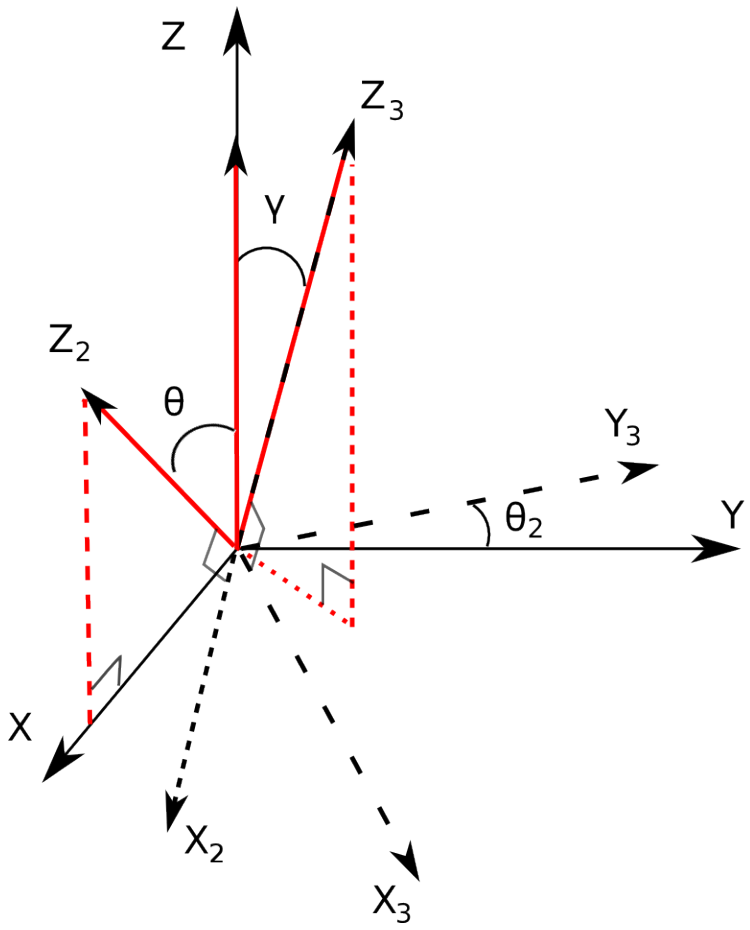

FIG. 3. Coordinate system chosen for the triple beam system.

C. Trap Analysis

To analyze the trap properties it is customary to fit a simple harmonic potential energy to the traps. We parameterize a line that runs through our interference pattern in a given direction and fit a simple harmonic potential energy to the simulated potential energy of the interference pattern along the line–that is we fit a curve of the form $U = 1/2\ m\omega_0^2 x^2$, where m is the mass of the atom being trapped, ω_0 is the natural angular frequency associated with the simple harmonic potential energy fit and x is the spatial displacement. This ω_0 gives us the trap frequency, f, which is equal to $\omega_0/2\pi$. A larger trap frequency corresponds to a more tightly bound atom in the trap. To further quantify the confinement of the fitted simple harmonic oscillator potential energy we calculate the size of the simple harmonic

wave function of the motional ground state along a spatial dimension j, as

$$\beta_j = \sqrt{\frac{\hbar}{2\pi f_j m}}, \tag{35}$$

for the $1/e$ half-width of the wave function's probability density where f_j is the trap frequency along that spatial dimension j, and m is the mass of the atom being trapped. We define the trap depth, ΔU_{trap}, as the difference between the peak of the fitted potential energy of the path of weakest confinement and the minimum of the potential energy well. The coherence of the qubits in a dipole trap is also limited by the scattering rate of trap photons. For blue-detuned traps the scattering rate for a ground state atom–averaged over the entire wave function–can be written as

$$\eta = \frac{\pi}{2}(f_w + f_s + f_3)\frac{\Gamma}{\Delta} + \frac{\Gamma}{\Delta\hbar}U_{min}, \tag{36}$$

where f_s is the frequency in the spatial dimension of strongest confinement in the x-z plane, f_w is the frequency in the spatial dimension of weakest confinement in the x-z plane, and f_3 is the frequency in the spatial y-dimension of the trap. All three directions are always orthogonal to one another. To account for a non-zero magnitude of intensity at the bottom of the well we add on the correction term containing U_{min}–the potential energy at the bottom of the well.

IV. RESULTS

A. Double Beam Trap

For two exactly equal beams with $\phi = 0$, linear polarization along y, $w_0 = 0.1$ mm, laser powers of P=10 W–corresponding to $I_0 = (2P)/(\pi w_0^2) \approx 6.37 \times 10^8$ W/m^2–and an angular displacement of $\pi/2$ between the propagation directions of the beams we calculate the interference pattern and the potential energy for the $F = 1, m_F = -1$ quantum state of ^{87}Rb–all following calculated potential energies are those of ^{87}Rb. It should be noted that the potential energy is equal for all possible F, m_F configurations unless the pattern exhibits some circular polarization. We plot the intensity viewed from the positive y-direction at y = 0 m in Fig. 4. We use a detuning of 1,000Γ, and a wavelength of λ = 780 (nm) in all examples. We calculate the potential energy and plot it viewed from the same perspective as the intensity plots–see Fig. 5

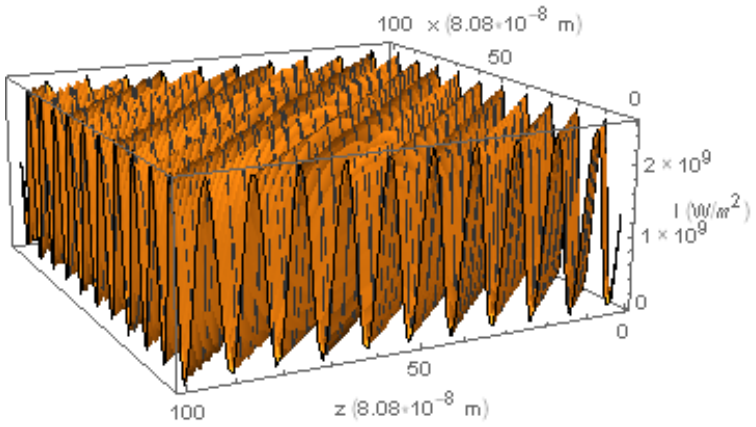

FIG. 4. Plot of the trap intensity in $\mathrm{W/m^2}$ as seen from the positive y-direction in the $x-z$ plane at $\theta = \pi/2$ with y=0.

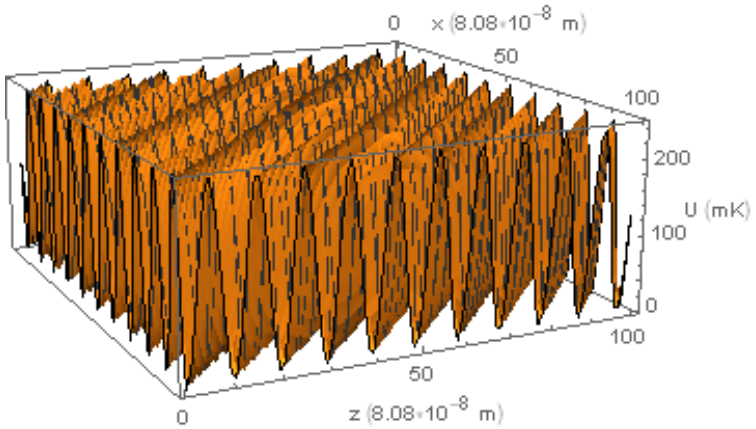

FIG. 5. Plot of the potential energy in mK for the $F = 1$, $m_F = -1$ quantum state as seen from the positive y-direction in the $x-z$ plane at $\theta = \pi/2$ with y=0.

For this case of equal beams we find that we yield nodal planes along the $x = z$ direction and that confinement is strong ($\Delta U_{trap} = 242$ mK). In the $x = -z$ direction and along the y-direction , however, we find that there is no confinement. See Fig.s 6 and 7 for plots of the intensity and potential energy in the $x-y$ plane at $z = 0$ m.

Plot of Potential Energy for Two Equal Beams

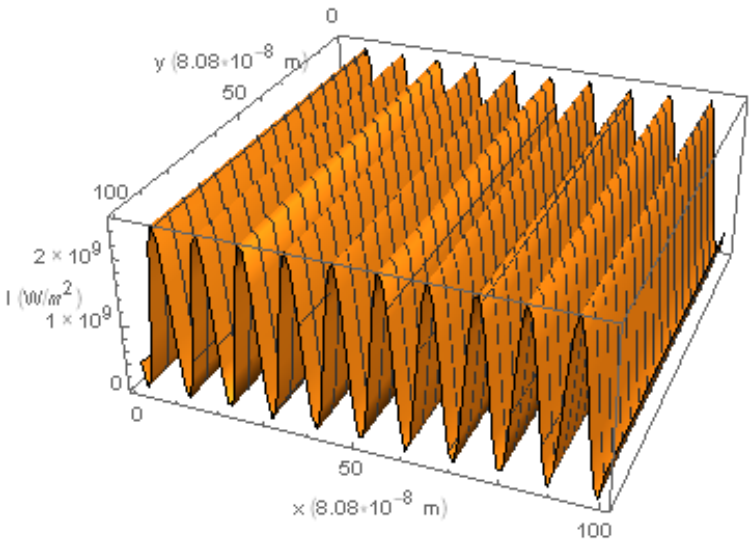

FIG. 6. Plot of the potential energy in mK for the $F = 1$, $m_F = -1$ quantum state as seen from the positive y-direction in the $x - y$ plane at $\theta = \pi/2$ with z=0.

Plot of Potential Energy for Two Equal Beams

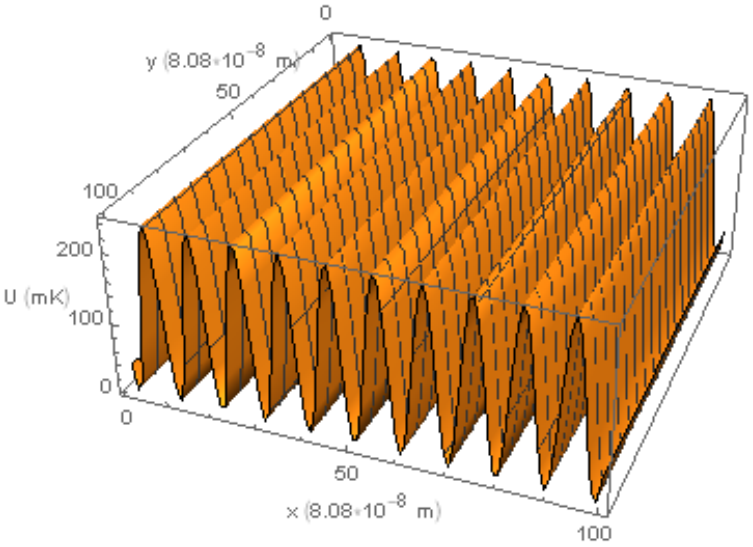

FIG. 7. Plot of the potential energy in mK for the $F = 1$, $m_F = -1$ quantum state as seen from the positive z-direction in the $x - y$ plane at $\theta = \pi/2$ with z=0.

Next, we investigate the instance that our beams are circularly polarized. To circularly polarize our beams we introduce a phase difference of $\pi/2$ between each beams' electric field's x-component and y-component with respect to their corresponding coordinate sys-

tems. Thus $\phi_{x1} = \phi_{x2} = 0$, and $\phi_{y1} = \phi_{y2} = \pi/2$, where the number 1 corresponds to the basis beam and the number 2 corresponds to the differential beam. We polarize our beams along $x = y$ for each beam's respective coordinate system to see the effects most distinctly. We plot the instance of two equal beams with these polarization angles, and the right circularly polarized beams–see Figs. 8, 9, 10, and 11 for intensity plots and potential energy plots at $\theta = \pi/2$.

Plot of Intensity for Equal Beams

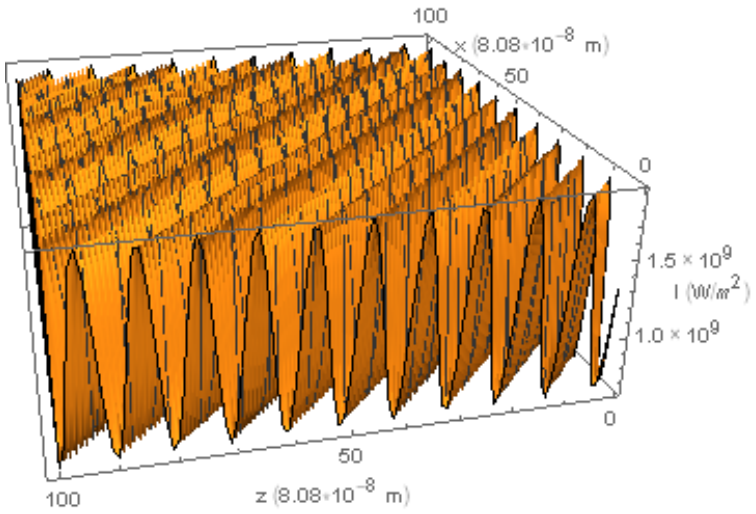

FIG. 8. Plot of the intensity pattern as seen from the positive y-direction in the $x - z$ plane with each beam being equal.

Plot of Potential Energy for Equal Beams

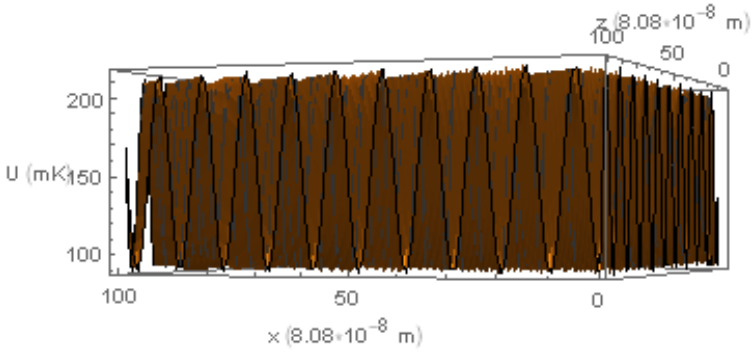

FIG. 9. Plot of the potential energy as seen from the positive y-direction in the $x - z$ plane with each beam being equal for the F=1, m_F=-1 quantum state.

Plot of Intensity for Right Circularly Polarized Beams

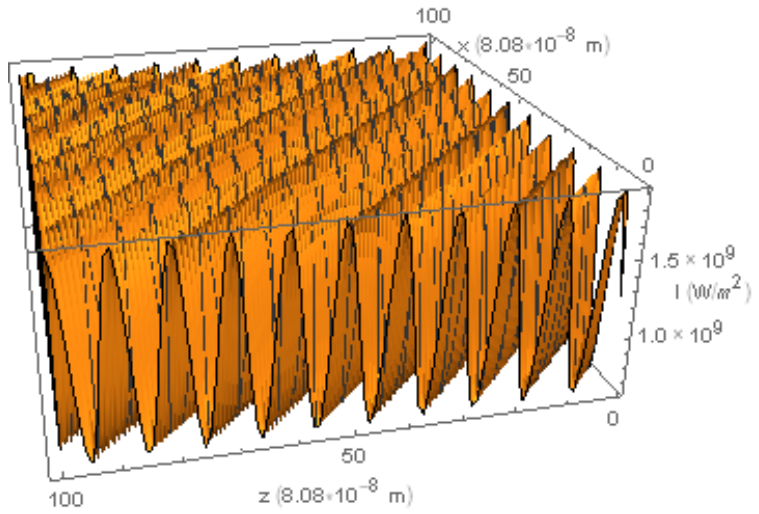

FIG. 10. Plot of the intensity pattern as seen from the positive y-direction in the $x-z$ plane with each beam being right circularly polarized.

Plot of Potential Energy for Right Circularly Polarized Beams

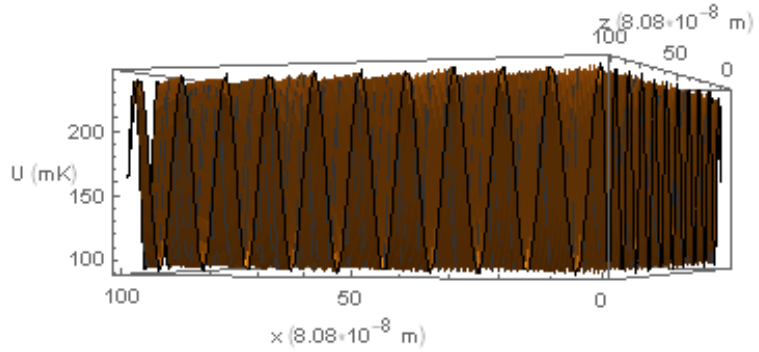

FIG. 11. Plot of the potential energy as seen from the positive y-direction in the $x-z$ plane with each beam being right circularly polarized for the F=1, m_F=-1 quantum state.

We find that the intensity pattern for this circularly polarized case is identical to the linear case, and that in the F=1, m_F=-1 quantum state the atoms are confined more in the right circularly polarized case than in the linearly polarized case–with ΔU_{trap} being closer to 200 mK than 100 mK.

To confine the third spatial dimension in our traps we introduce a difference in beam waist between the beams. We set $w_0 = 0.1$ mm for the basis beam and $w_0 = 0.01$ mm for the differential beam. We match the center intensity of the beams by decreasing the laser power of the differential beam 100 fold to 0.1 W. We plot both the intensity and potential in Figs. 12, and 13.

Plot of Intensity for Beams with Differing Beam Waists

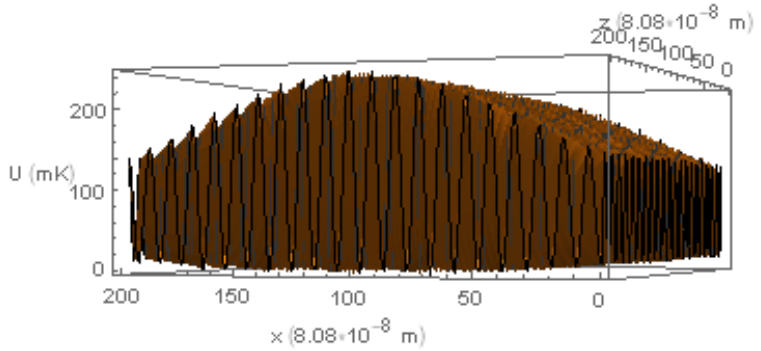

FIG. 12. Plot of the intensity pattern as seen from the positive y-direction in the $x - z$ plane with each beam having a different beam waist at $\theta = \pi/2$ and $y = 0$ m.

Plot of Potential Energy for Beams with Differing Beam Waists

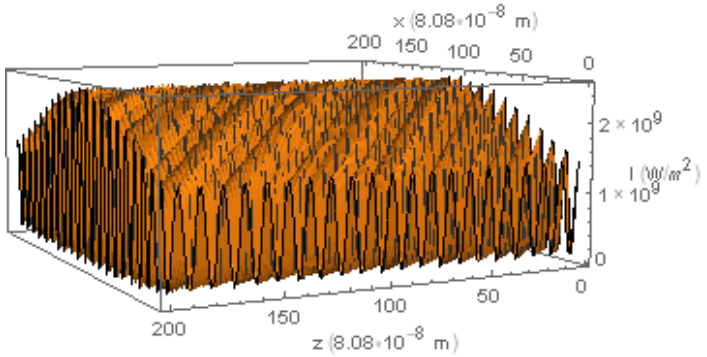

FIG. 13. Plot of the potential energy as seen from the positive y-direction in the $x - z$ plane with each beam having a different beam waist at $\theta = \pi/2$ and $y = 0$ m.

In the case of differing beam waist we find that there is a general curvature associated with the intensity and potential energy plots. An overall convexity in curvature in the $x = -z$ direction is attributed with an interference pattern closer to the origin whereas an overall concavity is apparent with larger y positions. This is because at these larger distances we

are sufficiently close to the "wall" of light created by the difference in beam waists–thus creating three dimensional confinement. We display this change in curvature in Fig. 14.

Plot of Potential Energy Data for Beams with Differing Beam Waists

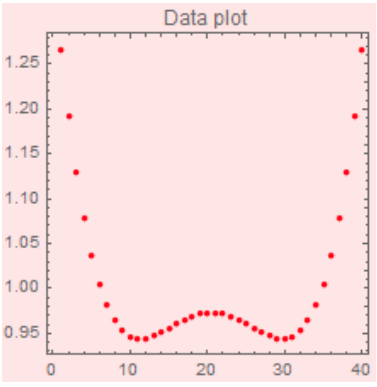

FIG. 14. Potential energy data along the weak direction at $\theta = \pi/2$ with the vertical axis in mK and the horizontal axis in units of 5.71×10^{-7} m/step.

To characterize the trapping properties of this pattern we parameterize lines traveling along the strongest dimension of the traps–i.e. $z = x$–the weakest dimension of the traps–i.e. $z = -x$–and a line in the y direction traveling through the bottom of a trapping plane. We fit our potential energy wells using Mathematica's fitting method. We do two sets of fits: one being aimed towards atoms of Bose-Einstein condensate (BEC) temperatures, and the other aimed towards atoms of MOT temperatures. Fig. 15 is the fit along the strongest dimension for both cases listed above, Fig. 16 is the fit along the y direction for the BEC instance, and Fig. 17 is the fit in the weakest dimension for the BEC instance. It should be noted that the bottom of the wells shown are closer to zero than the plots indicate–the nonzero values of the bottom of the wells and the value fluctuations amongst plots is attributed to the finite resolution of our calculated potential energies.

Simple Harmonic Oscillator Potential Energy Fits to Calculated Potential Energy

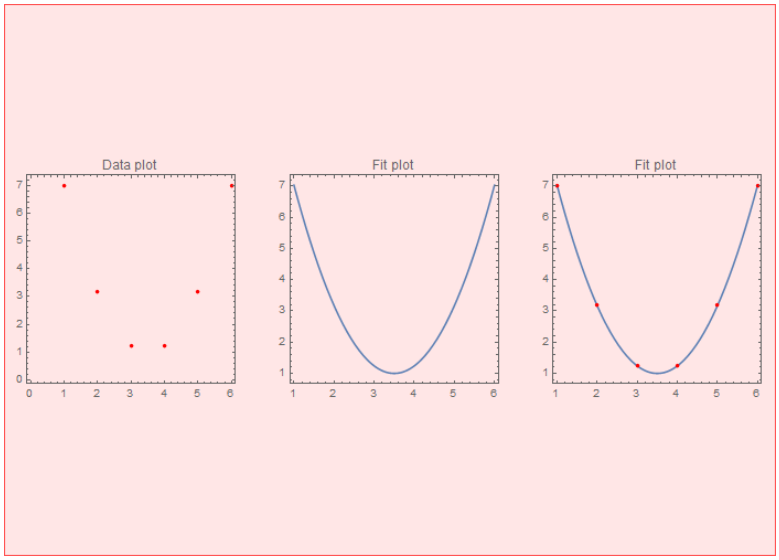

FIG. 15. Simple harmonic oscillator potential energy fits to calculated potential energy for the double beam system in the strong dimension at $\theta = \pi/2$ with the vertical axis in mK and the horizontal axis in units of 5.71×10^{-7} m/step.

Simple Harmonic Oscillator Potential Energy Fits to Calculated Potential Energy

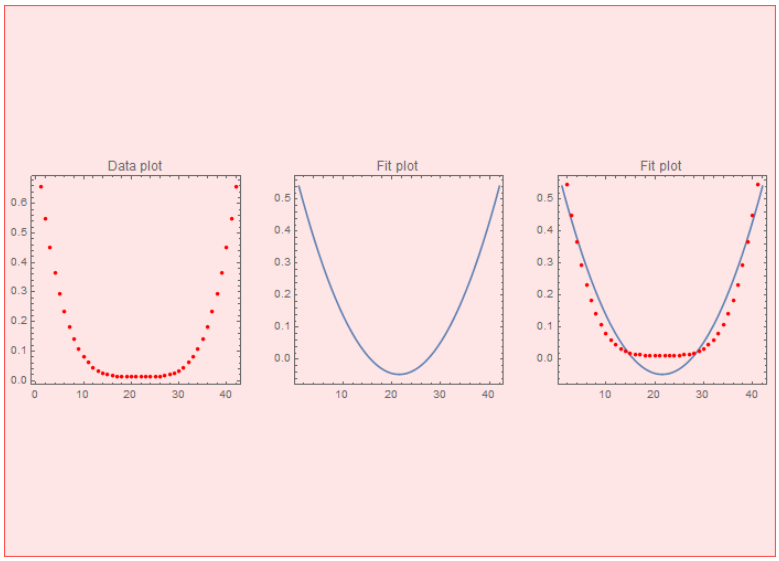

FIG. 16. Simple harmonic oscillator potential energy fits to calculated potential energy for the double beam system in the y-direction at $\theta = \pi/2$ with the vertical axis in mK and the horizontal axis in units of 5.71×10^{-7} m/step.

Simple Harmonic Oscillator Potential Energy Fits to Calculated Potential Energy

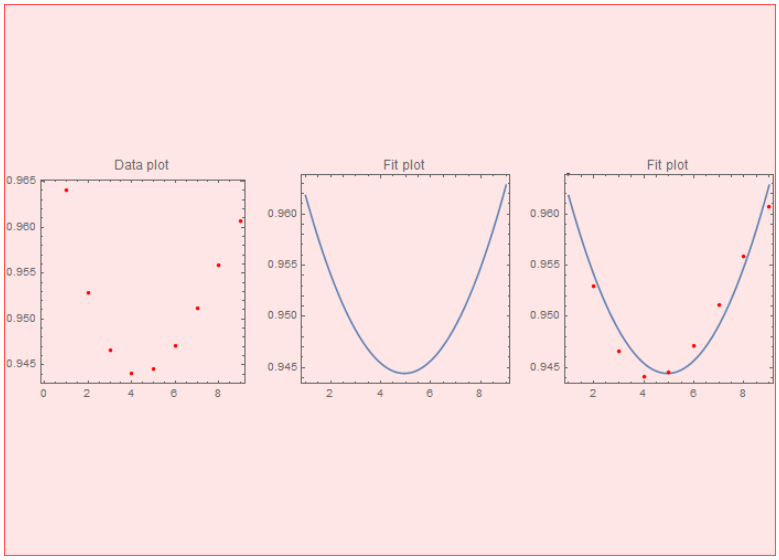

FIG. 17. Simple harmonic oscillator potential energy fits to calculated potential energy for the double beam system in the weak dimension at $\theta = \pi/2$ with the vertical axis in mK and the horizontal axis in units of 5.71×10^{-7} m/step.

We find the trapping frequencies and ground state sizes and list them in Table I. With these values we calculate a scattering rate of 41.8 KHz and a trap depth of 0.042 mK.

TABLE I. Trapping Parameters for the Potential Energy Pattern of the Beams with Different Beam Waists at $\pi/2$ for BEC atoms.

Direction	β (nm)	f (MHz)
$x = z$	2.14	25.29
$-x = z$	11.6	0.86
y	9.56	1.27

For the MOT atoms we find the fits for the wells on a larger scale as they are hotter than the BEC atoms. Figs. 18 and 19 show the fits in the weak dimension and the y-direction respectively.

Simple Harmonic Oscillator Potential Energy Fits to Calculated Potential Energy

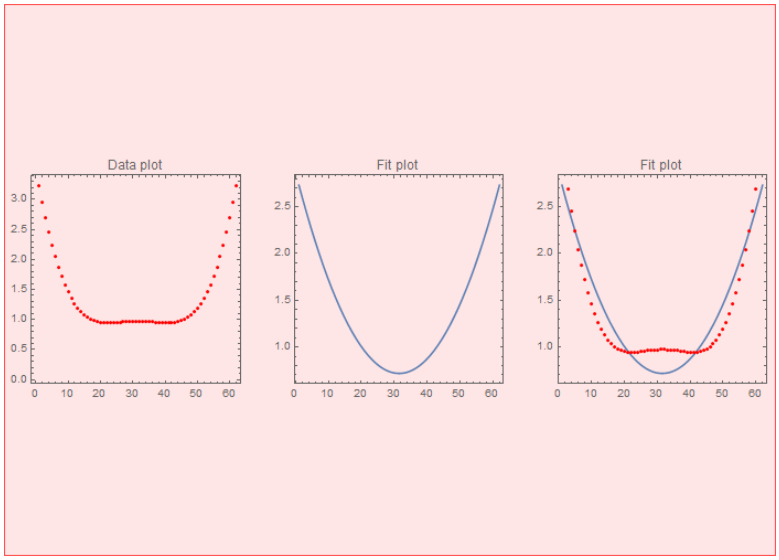

FIG. 18. Simple harmonic oscillator potential energy fits to calculated potential energy for the double beam system in the y-direction at $\theta = \pi/2$ with the vertical axis in mK and the horizontal axis in units of 5.71×10^{-7} m/step.

Simple Harmonic Oscillator Potential Energy Fits to Calculated Potential Energy

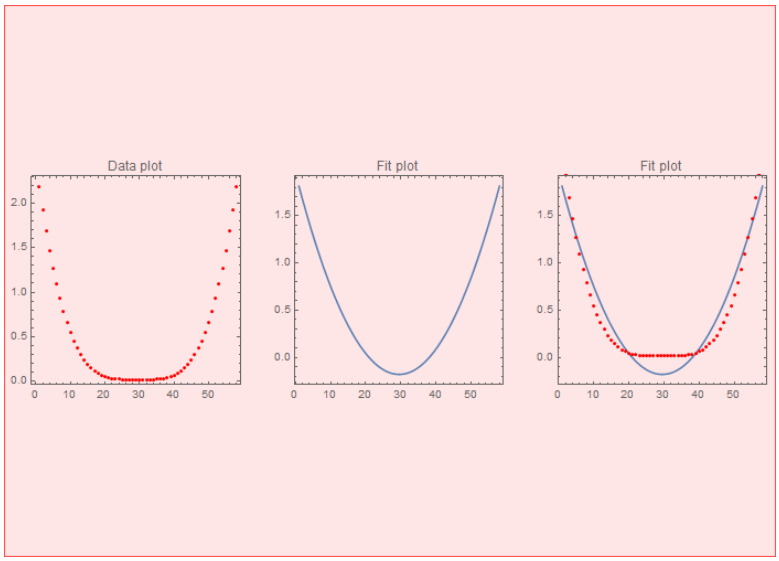

FIG. 19. Simple harmonic oscillator potential energy fits to calculated potential energy for the double beam system in the weak dimension at $\theta = \pi/2$ with the vertical axis in mK and the horizontal axis in units of 5.71×10^{-7} m/step.

We find the trapping frequencies and ground state sizes and list them in Table II.

TABLE II. Trapping Parameters for the Potential Energy Pattern of the Beams with Different Beam Waists at $\pi/2$ for MOT atoms.

Direction	β (nm)	f (MHz)
$x = z$	2.14	25.29
$-x = z$	18.3	0.35
y	13.8	0.61

With these values we calculate a scattering rate of 41.2 KHz and a trap depth of 12.4 mK.

B. Triple Beam Trap

To gain some intuition as to how the interference pattern of a triple beam system changes with varying γ, θ, and θ_2 we make several animations. For the instance of variable γ with $\theta = \pi/2$ and $\theta_2 = 0$ see gif 1 (a schematic of the beam dynamics is shown in Fig. 20), $\gamma = \pi/4$, $\theta_2 = \pi/4$, and variable θ is shown in gif 2 (a schematic of the beam dynamics is shown in Fig. 21), and $\gamma = \pi/4$, $\theta = \pi/2$, and variable θ_2 is shown in gif 3 (a schematic of the beam dynamics is shown in Fig. 22)–all gifs can be found the gifs folder. We also create an animation of the potential energy for the $F = 2$, $m_F = 2$ quantum state where $\gamma = \pi/2$, $\theta_2 = \pi/2$, and variable θ in gif 4 (a schematic of the beam dynamics is shown in Fig. 23). In each case the varying angle is evolving from 0 to 2π.

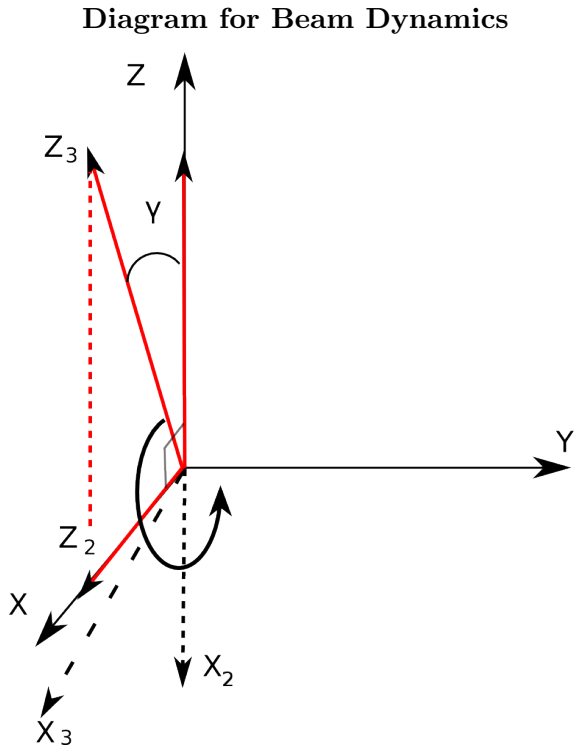

FIG. 20. Schematic for variable γ with $\theta = \pi/2$ and $\theta_2 = 0$.

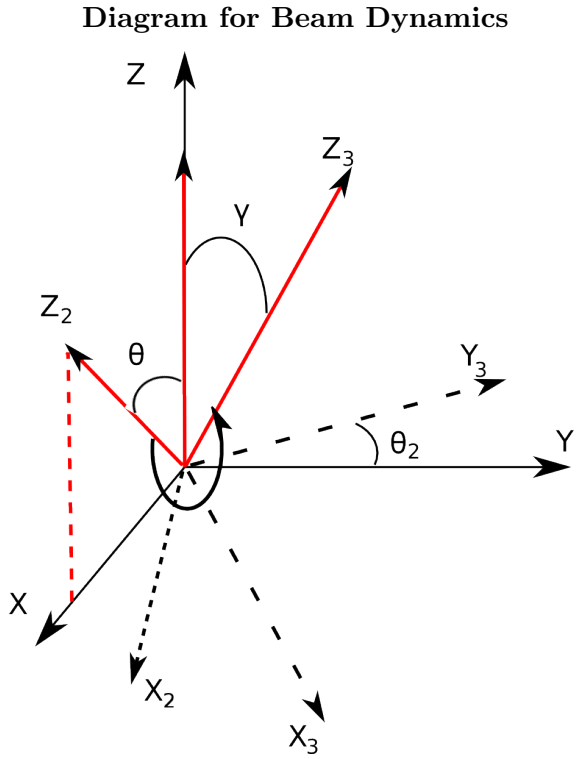

FIG. 21. Schematic for $\gamma = \pi/4$, $\theta_2 = \pi/4$, and variable θ.

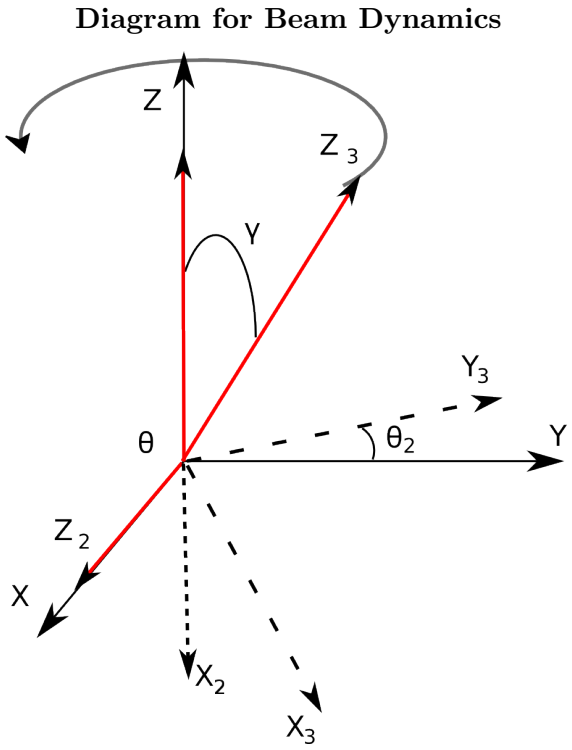

FIG. 22. Schematic for $\gamma = \pi/4$, $\theta = \pi/2$, and variable θ_2.

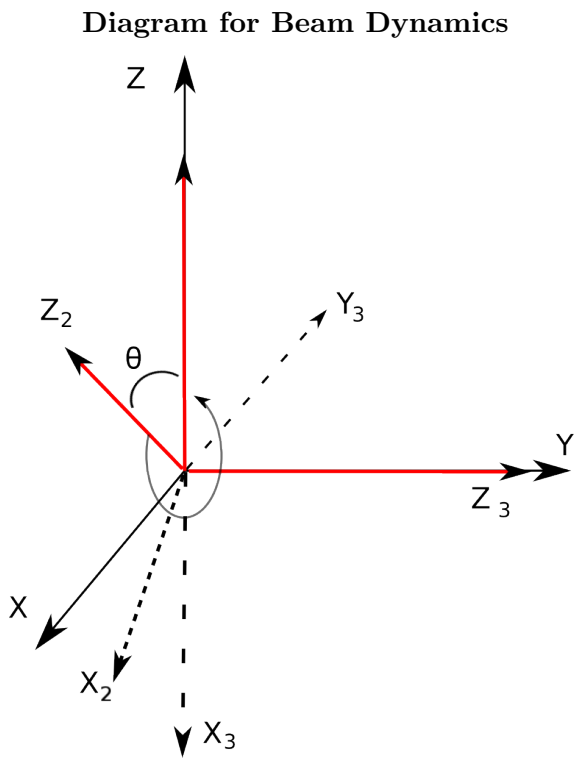

FIG. 23. Schematic for $\gamma = \pi/2$, $\theta_2 = \pi/2$, and variable θ.

To investigate the trapping properties of our triple beam system we, again, calculate the potential energy and fit a simple harmonic potential energy to some trap locations. For the instance of three equal beams with laser powers of 0.10 W, $w_0 = 0.1$ mm, $y = 0$ m, and linear polarization with $\theta = \pi/2$, $\gamma = 3\pi/4$, and $\theta_2 = 0$, we plot the potential energy from the positive and negative y-directions in the $x - z$ plane in Fig.s 24 and 25 respectively.

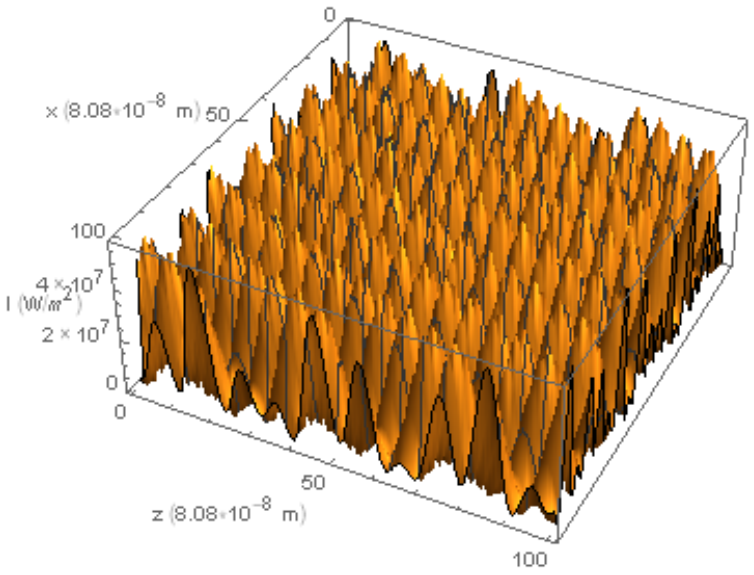

FIG. 24. Plot of the intensity pattern as seen from the positive y-direction in the $x-z$ plane with $\theta = \pi/2$, $\gamma = 3\pi/4$, and $\theta_2 = 0$.

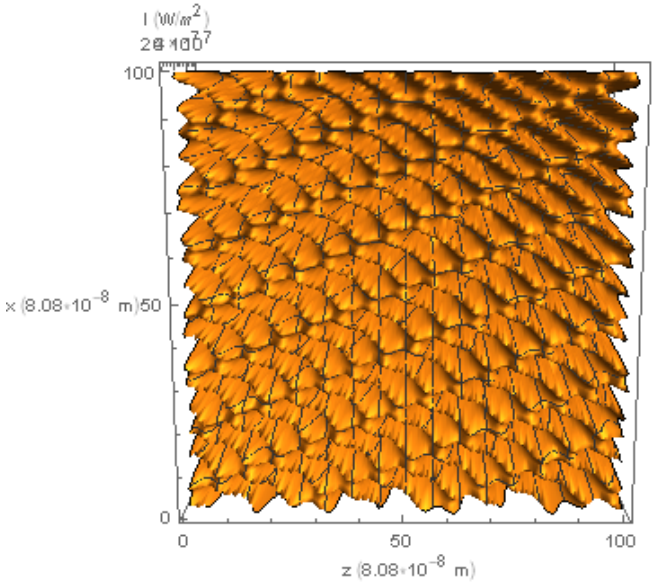

FIG. 25. Plot of the intensity pattern as seen from the negative y-direction in the $x-z$ plane with $\theta = \pi/2$, $\gamma = 3\pi/4$, and $\theta_2 = 0$.

We parameterize lines traveling along the three dimensions of the trap: the strongest dimension–i.e. $x = z$–the weakest being $-x = z$, and the y direction. We fit our potential energy wells in these three dimensions using the series method and the least squares fitting method–see Fig. 26. for the $x = y$ fit, Fig. 27 for the z direction fit, and Fig. 28 for the

$x = -z$ fit.

Simple Harmonic Oscillator Potential Energy Fits to Calculated Potential Energy

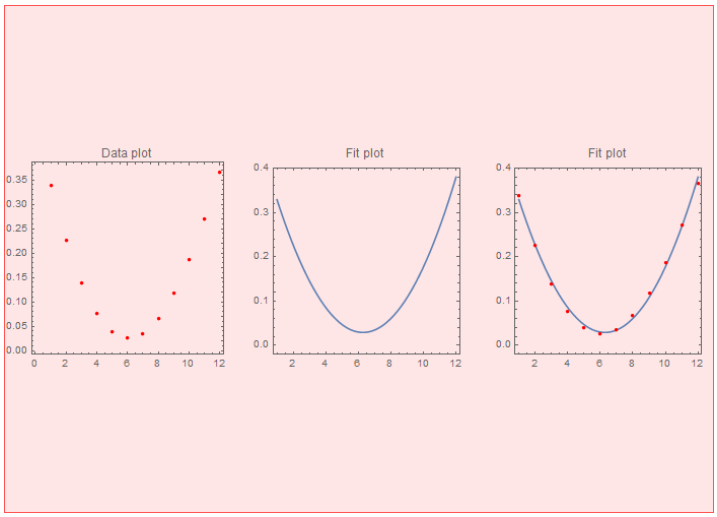

FIG. 26. Simple harmonic oscillator potential energy fits to calculated potential energy of our triple beam system along $x = z$ with $\theta = \pi/2$, $\gamma = 3\pi/4$, and $\theta_2 = 0$ with the vertical axis in mK and the horizontal axis in units of 5.71×10^{-7} m/step.

Simple Harmonic Oscillator Potential Energy Fits to Calculated Potential Energy

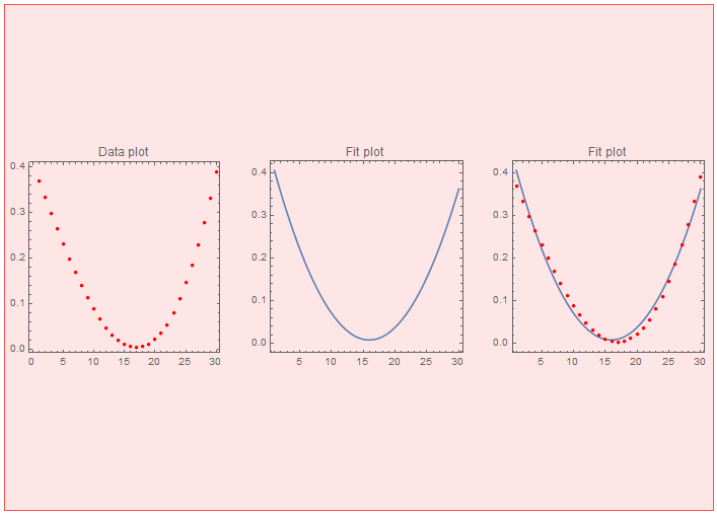

FIG. 27. Simple harmonic oscillator potential energy fits to calculated potential energy for the triple beam system along the y direction with $\theta = \pi/2$, $\gamma = 3\pi/4$, and $\theta_2 = 0$ with the vertical axis in mK and the horizontal axis in units of 5.71×10^{-7} m/step.

Simple Harmonic Oscillator Potential Energy Fits to Calculated Potential Energy

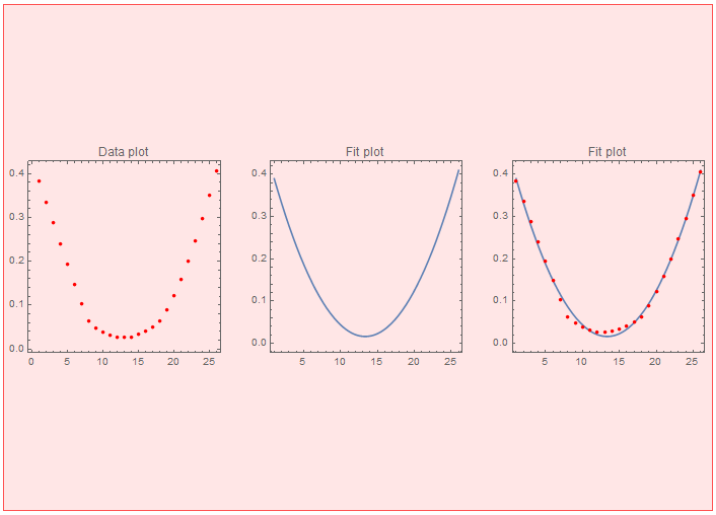

FIG. 28. Simple harmonic oscillator potential energy fits to calculated potential energy for the triple beam system along $x = -z$ direction with $\theta = \pi/2$, $\gamma = 3\pi/4$, and $\theta_2 = 0$ with the vertical axis in mK and the horizontal axis in units of 5.71×10^{-7} m/step.

We find the trapping frequencies and ground state sizes and list them in Table II.

TABLE III. Trapping Parameters for the Potential Energy Pattern of the Triple Beam System at $\theta = \pi/2$, $\gamma = 3\pi/4$, and $\theta_2 = \pi/2$.

Direction	β (nm)	f (MHz)
$x = z$	6.60	2.66
$-x = z$	9.55	1.27
y	10.3	1.08

With these values we calculate a scattering rate of 8.00 KHz, and a trap depth of 0.62 mK.

C. Entanglement

For the triple beam trap we investigate how information may propagate through the interference pattern. Bringing two trapped atoms close to one another we may entangle their wave functions by pulsing both of them with a laser beam. If we then take one of these two entangled qubits and entangle it with another qubit we propagate entanglement from qubit 1 to qubit 3 or from qubit 2 to qubit 3. For us to channel entanglement through our system we must be able to entangle qubits in a logical sequence. We analyze the case where we vary γ with $\theta = \pi/2$ and $\theta_2 = 0$ as seen in gif 2. We oscillate the value of γ between $3\pi/4$ and $7\pi/4$ to translate qubit entanglement diagonally along the edges of the hexagonal interference structure shown by the black line drawn in Fig. 29.

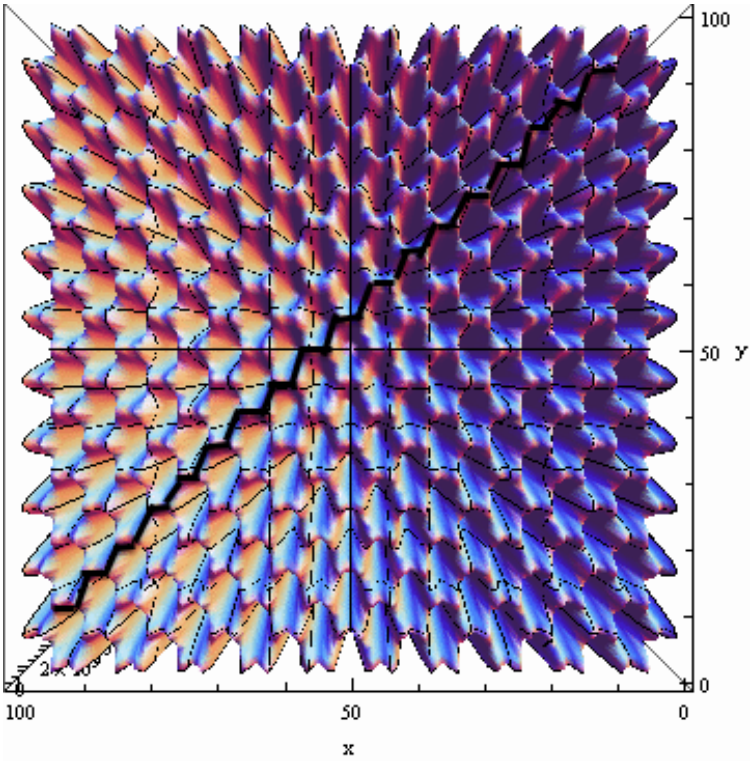

FIG. 29. How entanglement would propagate through the interference pattern by oscillating γ between $3\pi/4$ and $7\pi/4$ (γ=π).

We start at our maximum γ and entangle the two trapped atoms (each well is assumed to contain one trapped atom each) indicated by the circle in Fig. 30. By decreasing γ to $3\pi/4$ we then separate the two entangled atoms and bring them together with two different trapped atoms–indicated by the circles in Fig. 31. With appropriate laser pulses we can

pass entanglement to these two atoms. If we continue to increase γ back to our maximum value the two newly entangled atoms could have their entanglement passed on to two more new atoms along the diagonal. We continue this oscillation of γ until the entanglement has propagated to the intended qubit, even if they reside far away from each other in the trap array.

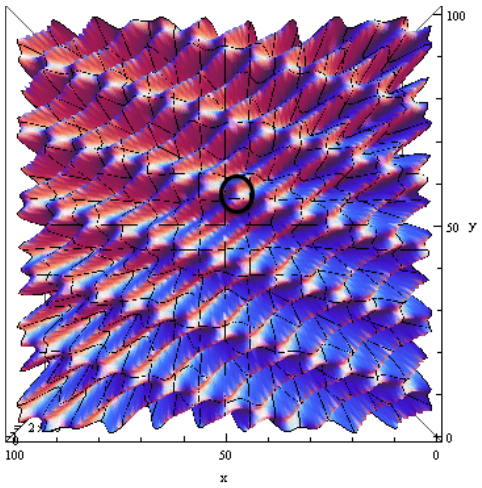

FIG. 30. Initial location of the two atoms being entangled with one another at $\gamma = 7\pi/4$.

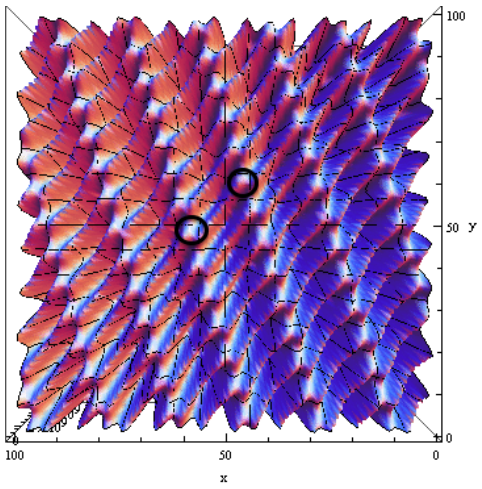

FIG. 31. Final locations of the two entangled atoms–now able to entangle with two new atoms at $\gamma = 3\pi/4$

Propagating entanglement in our trap array allows us to complete logical gate operations on various qubits in our system–allowing us to complete quantum computations.

V. CONCLUSION

We proposed two optical neutral atom trap arrays involving the intersection of two or three laser beams. We investigated the nature of our double beam trap by analyzing how the intensity pattern and calculated potential energy changed with varying beam waist, and beam polarization. By fitting simple harmonic energies to the interference pattern's calculated potential energy we were able to characterize the traps by their trap frequencies–and thus their scattering rates–and their motional ground state sizes. By inspecting our potential energy plots we were able to determine the trap depths. For the case of the double beam trap with different beam waists at $\theta = \pi/2$, we found $\eta = 41.8$ KHz and and ΔU_{trap} $= 0.042$ mK for BEC atoms, and $\eta = 41.2$ KHz and $\Delta U_{trap} = 12.4$ mK for MOT atoms. For the case of the triple beam trap with all beams having equal parameters at $\theta = \pi/2$, $\theta_2 = 0$, and $\gamma = 3\pi/4$ we found $\eta = 8.00$ KHz and $\Delta U_{trap} = 0.62$ mK. We created animations to analyze how the potential energy and intensity changed with varying angles of separation between the laser beams in the system. Finally we highlighted a possible atom entanglement routine by oscillating the polar angle, γ, in our triple beam system between $3\pi/4$ and $7\pi/4$ and discussed how entanglement would propagate through the system.

ACKNOWLEDGMENTS

I would like to acknowledge my mentor Katharina Gillen for her invaluable advice and guidance, and Travis Fraser for his tremendously helpful programs that I adapted for my work.

---

[1] David P. DiVincenzo, "The physical implementation of Quantum Computation" Fortschritte der Physik **48**(9-11), 771-783 (2000).

[2] Ashkin, A., "Acceleration and trapping of particles by radiation pressure" Phys. Rev. 24, 156-159 (1970).

[3] M. D. Wang, H. Yin, R. Landick, J. Gelles, and S. M. Block "Streching DNA with optical tweezers." Biophys J. 72 **3**, 1335-1346 (1997).

[4] Rudolf Grimm and Matthias Weidemüller "Optical Dipole Traps For Neutral Atoms" Advances in Atomic, Molecular and Optical Physics **42**, 95-170 (2000).

[5] Glen D. Gillen, Shekhar Guha, and Katharina Christandl "Optical dipole traps for cold atoms using diffracted laser light" Phys. Rev. A **73**, 013409 (2006).

[6] Katharina Gillen-Christandl and Bert D. Copsey "Polarization-dependant atomic dipole traps behind a circular aperture for neutral-atom quantum computing" Phys. Rev. A **83**, 023408 (2011).

[7] Frank L. Pedrotti, Leno M. Pedrotti, and Leno S. Pedrotti, *Introduction to Optics* 3rd Ed., Addison-Wesley (2006-04-17).

VI. APPENDIX

Assuming that the basis beam lies completely along the z-axis and defines our coordinate basis we write

$$E_1 = E_{1x}\hat{i} + E_{1y}\hat{j}, \tag{37}$$

because the electric field is prohibited from pointing in the direction of beam propagation. Our first differential beam subtends and angle θ with the basis beam and lies in the $x - z$ plane (see Fig. 32)–thus we write out its electric field in terms of the basis coordinate system as

$$E_2 = E_{2x}cos(\theta)\hat{i} + E_{2y}\hat{j} + E_{2x}sin(\theta)\hat{k}. \tag{38}$$

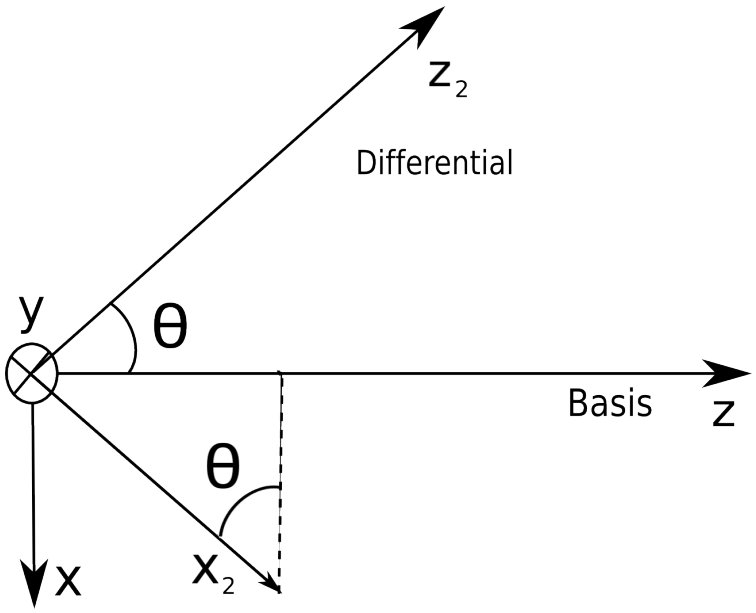

FIG. 32. Diagram of the double beam coordinate system and the electric field component's projections.

The second differential beam subtends a polar angle of γ with respect to the basis beam and is rotated about an azimuthal angle of θ_2. Using the convention that the y_3-component of the second differential beam lies completely the $x-y$ plane we can determine it's projections of it's electric field components on the basis axes.

The second differential beam's electric field components written in terms of the coordinate basis can be determined entirely by the projections of the x_3-and y_3-axes onto our basis axes

as there is no electric field component in the direction of propagation (the z_3-direction). x_3's radial projection is given as $x_3\cos(\gamma)$ (see Fig. 33 for a visual reference).

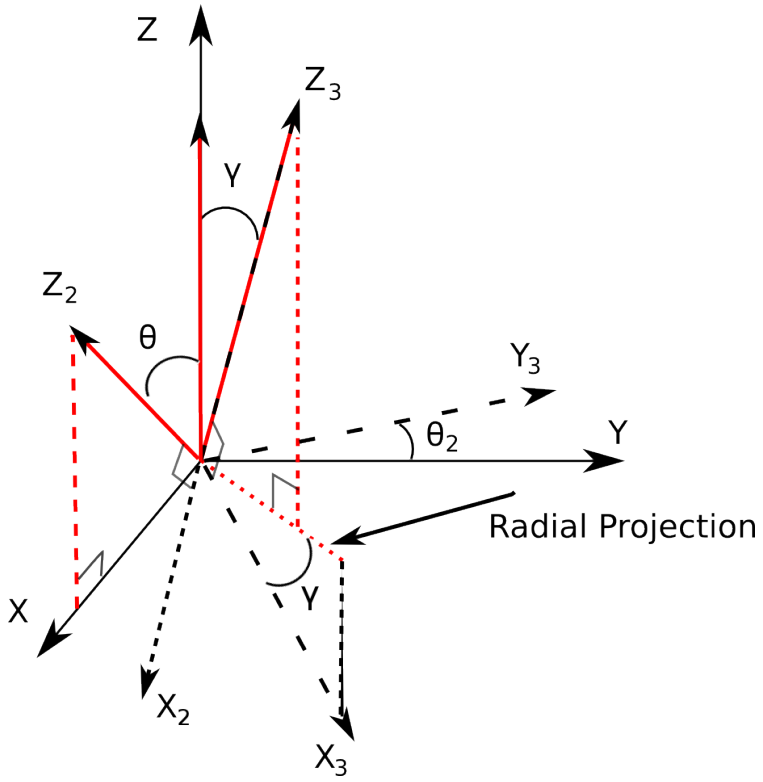

FIG. 33. Diagram of the triple beam coordinate system and the x_3-component's projection.

Thus its projection along y is $x_3\cos(\gamma)\sin(\theta_2)$, whereas y_3's projection along y is given as $y_3\cos(\theta_2)$. Replacing the coordinates x_3 and y_3 with the electric field components E_{3x} and E_{3y} and taking a superposition of the electric field components from the other beams in this direction results in the expression:

$$E_y = E_{1y}(x,y,z) + E_{2y}(x_2,y_2,z_2) + E_{3x}(x_3,y_3,z_3)cos(\gamma)sin(\theta_2) + E_{3y}cos(\theta_2). \quad (39)$$

Similarly we take the projections of x_3 and y_3 along the x-axis to yield

$$E_x = E_{1x}(x,y,z) + E_{2x}(x_2,y_2,z_2)cos(\theta) + E_{3x}(x_3,y_3,z_3)cos(\theta_2)cos(\gamma) - E_{3y}sin(\theta_2). \quad (40)$$

Finally, the only component of the electric field in the z-direction is given as the projection of x_3 along z, hence

$$E_z = E_{2x}(x_2,y_2,z_2)sin(\theta) + E_{3x}(x_3,y_3,z_3)(-sin(\gamma)). \quad (41)$$